Article

A phospholipid-biomimetic fluorescent mitochondrial probe with ultrahigh selectivity enables in-situ and high-fidelity tissue imaging

Ruoyao Zhang, Yuming Sun, Minggang Tian, Ge Zhang, Ruiqing Feng, Xuechen Li, Lifang Guo, Xiaoqiang Yu, Jing Zhi Sun, and Xiuquan He

Anal. Chem., **Just Accepted Manuscript** • Publication Date (Web): 17 May 2017

A phospholipid-biomimetic fluorescent mitochondrial probe with ultrahigh selectivity enables *in-situ* and high-fidelity tissue imaging

Ruoyao Zhang,[†] Yuming Sun,[‡] Minggang Tian,[†] Ge Zhang,[†] Ruiqing Feng,[†] Xuechen Li,[†] Lifang Guo,[†] Xiaoqiang Yu,*[,†] Jing Zhi Sun*[,§] and Xiuquan He*[,∥]

[†]Center of Bio & Micro/Nano Functional Materials, State Key Laboratory of Crystal Materials, Shandong University, Jinan 250100, P. R. China. Fax: +86 0531 88364263; E-mail address: yuxq@sdu.edu.cn

[‡]School of Information Science and Engineering, Shandong University, Jinan 250100, P. R. China

[§]MoE Key Laboratory of Macromolecule Synthesis and Functionalization, Department of Polymer Science and Engineering, Zhejiang University, Hangzhou 310027, P. R. China. Fax: +86 0571 87953734; E-mail address: sunjz@zju.edu.cn

[∥]Department of Anatomy, Shandong University School of Medicine, Jinan 250012, P. R. China. Fax: +86 0531 88364263; E-mail address: hxq3000@sdu.edu.cn

ABSTRACT: *In-situ* and directly imaging mitochondria in tissues instead of isolated cells can offer more native and accurate information. Particularly, in the clinical diagnose of mitochondrial diseases such as mitochondrial myopathy, it is a routine examination item to directly observe mitochondrial morphology and number in muscle tissues from patients. However, it's still a challenging task because the selectivity of available probes is inadequate for exclusively tissue imaging. Inspired by the chemical structure of amphiphilic phospholipids in mitochondrial inner membrane, we synthesized a phospholipid-biomimetic amphiphilic fluorescent probe (**Mito-MOI**) by modifying a C_{18}-alkyl chain to the lipophilic side of carbazole-indolenine cation. Thus the phospholipid-like **Mito-MOI** locates at mitochondrial inner membrane through electrostatic interaction between its cation and inner membrane negative charge. Simultaneously, the C_{18}-alkyl chain, as the second targeting group, is deeply embedded into the hydrophobic region of inner membrane through hydrophobic interaction. Therefore, the dual targeting groups (cation and C_{18}- alkyl chain) actually endow **Mito-MOI** with ultrahigh selectivity. As expected, high-resolution microscopic photos showed that **Mito-MOI** indeed stained mitochondrial inner membrane. Moreover, *in-situ* and high-fidelity tissue imaging has been achieved, and particularly, four kinds of mitochondria and their crystal-like structure in muscle tissues were visualized clearly. Finally, the dynamic process of mitochondrial fission in living cells has been shown. The strategy employing dual targeting groups should have reference value for designing fluorescent probes with ultrahigh selectivity to various intracellular membranous components.

Different from the microscopic images obtained in cultured cells, *in-situ* and directly imaging mitochondria in intact tissues can offer more native and accurate information.[1] On one hand, cells in living tissues are surrounded by native extracellular matrix (ECM) with indispensable functions compared to culture medium,[2,3] such as mediating tissue morphogenesis and providing clews for cell proliferation and differentiation.[4,5] On the contrary, cells cultured are often immortalized for infinite proliferation, which will damage their original differentiated functions.[6] More importantly, the change of mitochondrial morphology and number in muscle tissues have clinical diagnostic value in mitochondrial diseases, such as mitochondrial myopathy, encephalopathy, lactic acidosis, and stroke-like episodes (MELAS).[7-10] For example, in muscular tissues with MELAS, the smooth muscle cells of the succinate-dehydrogenase-reactive blood vessels show marked proliferation of mitochondria.[10] Thus it is a routine examination item to directly observe mitochondria in muscle tissues from patients and available observing method by scanning electron microscope (SEM) is complex.[7,9,10] However, it is still a challenging task to *in-situ* and directly image mitochondria in tissues by fluorescent microscopy due to the low selectivity of fluorescent probes available.

So far, available mitochondrial probes generally bear an organic cationic unit,[11-18] which enables them to target mitochondria with a negative membrane potential of -180 mV.[19-21] Generally, their selectivity to mitochondria is enough to image cells, but inadequate for tissue imaging. In tissues, the substances are far more complex than that in cells, such as various amounts of collagens, adhesion molecules, proteoglycans, growth factors and cytokines in ECM.[4,5] As a result, some probes are nonspecifically bound to other components and thus produce high background noise. When staining cells, the background fluorescence can be eliminated by washing out unbound probes,[22-24] while washing process cannot be adopted when staining living tissues. On the other hand, due to matured cell culture technology, the incubation time for staining cells is allowed for 0.5 hours or longer.[13, 25-27] However, the viability of isolated living tissues will rapidly decay and the mitochondrial membrane potential may also rapidly decrease. Hence, the staining time must be as short as possible. Thus, to image tissues, a probe with ultrahigh selectivity is urgent.

One possible and rational way is to design a probe with dual targeting groups. A key fact is that the tight bilayer of mitochondrial inner membrane mainly composes of amphiphilic phospholipids,[28,29] such as phosphatidylcholine and phospha-

tidyl ethanolamine, which contain a hydrophilic cation and hydrophobic overlong alkyl chains (Scheme 1a). Inspired by the chemical structure of phospholipids, we believe that the ultrahigh selectivity can be realized by a phospholipid-biomimetic amphiphilic mitochondrial probe prepared by modifying an overlong alkyl chain to the lipophilic side of a common cationic mitochondrial probe (Scheme 1a). According to Scheme 1b, the probes should be able to naturally and stably arrange in inner leaflet of mitochondrial inner membrane, like some phospholipids. In accordance with the orientation of amphiphilic phospholipids, the cations are located at the hydrophilic side of inner leaflet due to the electrostatic interaction with inner membrane negative charge. Simultaneously, the overlong alkyl chain, as the second targeting group, is embedded into the hydrophobic region of the inner leaflet through hydrophobic interaction. Therefore, compared with common cationic mitochondrial probes, this phospholipid-biomimetic probe has an additional hydrophobic interaction with mitochondria (Scheme 1b). As a result, the binding affinity can be obviously enhanced, which offers ultrahigh selectivity required by tissue imaging. However, a serious concern is that dyes with overlong alkyl chain most probably stay in plasma membrane. Interestingly, not all probes with overlong alkyl chains are hindered by plasma membrane. Another key fact is that plasma membrane probes bearing long chains sometimes show rapid internalization, such as Laurdan with a C_{12}-chain.[30] The two key facts tell us a crucial possibility that a mitochondrial probe simultaneously possessing ultrahigh selectivity and fast stainability can be synthesized by exquisitely introducing an overlong alkyl chain to common cationic mitochondrial probe.

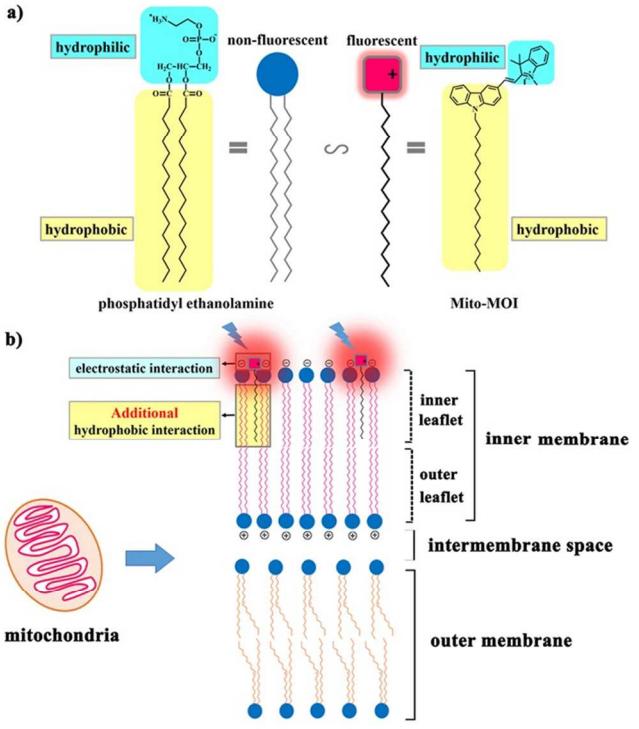

Scheme 1. Chemical structures of phosphatidyl ethanolamine and **Mito-MOI** (a), and binding model of **Mito-MOI** within mitochondrial inner membrane (b).

Herein, a probe **Mito-MOI** was synthesized by carefully modifying a C_{18}-alkyl chain to the lipophilic side of carbazole-indolenine cation (Scheme 2). The structure of **Mito-MOI** was characterized by ^{1}H NMR, ^{13}C NMR, IR and HRMS spectra, as showed in Supporting Information. As expected, **Mito-MOI** was able to light up mitochondria in living cells, and high resolution microscopic photos have shown that **Mito-MOI** exclusively stains mitochondrial inner membrane. Moreover, mitochondria in living tissues have been *in-situ* and high-fidelity imaged. Particularly, four kinds of mitochondria and their crystal-like structure in muscle tissues were also visualized clearly. Therefore, modifying a long alkyl chain to the lipophilic side of a cation was a reasonable choice to create a mitochondrial probe with ultrahigh selectivity.

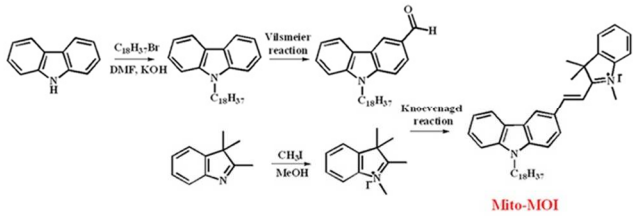

Scheme 2. The synthetic routines of **Mito-MOI**.

EXPERIMENTAL SECTION

Apparatus and general methods. The UV-visible-near-IR absorption spectra of dilute solutions were recorded on a HITACH U-2910 spectrophotometer using a quartz cuvette having 1 cm path length. One-photon spectra were obtained on a HITACH F-2700 spectrofluorimeter equipped with a 450-W Xe lamp. The mitochondrial probes MitoTracker Green (MTG) and MitoTracker Red (MTR), and double-stranded DNA-specific dye Hoechst 33342 were purchased from Molecular Probes. PBS buffer solution: 10 mM NaCl, Na_2HPO_4•$12H_2O$, NaH_2PO_4•$2H_2O$, pH = 7.40.

Measurement of Φ. Quantum yield (Φ) can be calculated by means of Eq. (1):[31]

$$\Phi_s = \Phi_r \frac{A_r \lambda_r n_s^2 F_s}{A_s \lambda_s n_r^2 F_r} \quad (1)$$

s and r refer to the sample and the reference materials, respectively. Φ is the quantum yield, F is the integrated emission intensity, A stands for the absorbance, and n is the refractive index. In this work, the quantum yields were calculated by using fluorescein (Φ = 0.95, pH = 13) as the standard.

Cell culture and staining. All cells were grown in a 5% CO_2 incubator at 37 ^{o}C. Human cervical cancer cell lines (SiHa and HeLa) were grown in Dulbecco's Modified Eagle Medium supplemented with 10% fetal bovine serum (FBS) and 1% penicillin and streptomycin. Rat astrocytes and neurons were cultured in Dulbecco's Modified Eagle Media: Nutrient Mixture F-12 supplemented with 10% bovine calf serum in a 5% CO_2 incubator at 37 °C. **Mito-MOI** was dissolved in DMSO at a concentration of 5 mM. Hoechst 33342 was prepared as 1 mM aqueous solution. MTG and MTR were dissolved in DMSO at a concentration of 0.1 mM. HeLa and SiHa cells were placed on glass coverslips and allowed to adhere for 24 h. Rat astrocytes were placed on glass coverslips and allowed to adhere for 6 days. For living cells imaging experiment of probes (**Mito-MOI**, MTG and MTR), cells were incubated with probes (**Mito-MOI**: 5 μM; MTG: 0.2 μM; MTR: 0.2 μM) in DMEM for 30 min (**Mito-MOI** for 5 min) at 37 °C. Every time (expect for the experiment of real-time observation), the cells were washed to remove the unbound

probe before stained with another probe. After rinsing with PBS twice, cells were imaged immediately.

Cell-viability assay: the study of the effect of **Mito-MOI** on viability of cells was carried out using the methylthiazolyldiphenyl-tetrazolium bromide (MTT) assay. HeLa and SiHa cells growing in log phase were seeded into 96-well plates (ca. 1×10^4 cells/well) and allowed to adhere for 24 h, respectively. **Mito-MOI** (200 μL/well) at concentrations of 10 μM, 5 μM, and 2.5μM was added into the wells of the treatment group, and 200 μL/well DMSO diluted in DMEM at final concentration of 0.2% to the negative control group, respectively. The cells were incubated for 24 h at 37 °C under 5% CO_2, respectively. Then MTT (5 mg/mL in DMEM) was added into each well. After 4 h incubation at 37 °C, 200 μL DMSO was added to dissolve the purple crystals. After 20 min incubation, the optical density readings at 492 nm were taken using a plate reader. Cytotoxic experiment was repeated for four times.

Tissue staining: the rat skeletal muscle, cardiac muscle and hepatic tissues were directly removed from just killed adult wistar rat (purchased from Laboratory Animal Center, Shandong University). Then they were stained with **Mito-MOI** (5 μM, 5 min) at room temperature in H-DMEM supplemented with 10% fetal bovine serum (FBS) and 1% penicillin and streptomycin.

Fluorescent imaging. Wide-field fluorescent images were acquired with an Olympus IX71 inverted microscope coupling with a CCD and display controller software. The fluorescence of **Mito-MOI** was excited and collected through the red channel. Confocal fluorescent images were obtained with a LSM 780 confocal laser scanning microscope or an Olympus FV 300 laser Confocal Microscope. The overlap coefficients and fluorescence intensity of the images were determined by the software with the LSM 780 confocal microscope. For the Olympus Microscope, emission was collected with a beam splitter DM570 and an IF565 nm pass filter combination.

RESULTS AND DISCUSSION

Photophysical properties. The absorption and fluorescence spectra of **Mito-MOI** have been plotted in Figure 1. At the same time, the relevant photophysical parameters of **Mito-MOI** have been summarized in Table S1. From Table S1, one

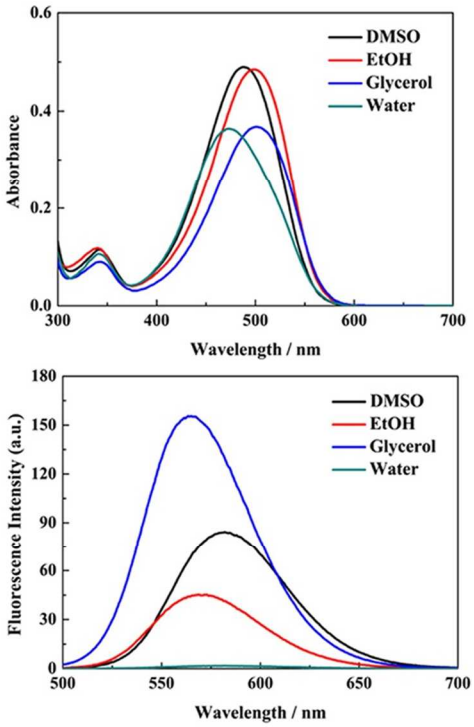

Figure 1. Absorption and fluorescence spectra of **Mito-MOI** in DMSO, EtOH, glycerol and water. Excited wavelengths: the corresponding maximum absorption wavelengths. Compound concentration: 10 μM.

can find that Φ value of **Mito-MOI** is very low in aqueous solutions, and turns larger in some organic solvents. It should be noted that the Φ value is obviously enhanced in glycerol, an organic solvent with rather high viscosity, which should be attributed to the restrain of its intramolecular motions. Since **Mito-MOI** can target mitochondrial inner membrane which can also provide high-viscosity conditions,[15] this physical property of the probe greatly favors its imaging of mitochondria with high-fidelity.

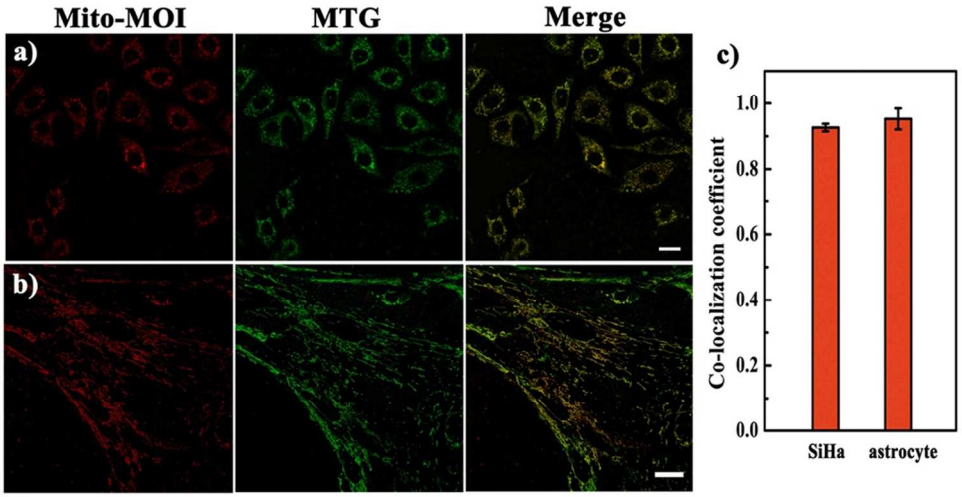

Figure 2. Confocal fluorescent images of SiHa (a) and astrocytes (b) stained with **Mito-MOI** (5 μM, 5 min) and MTG (0.2 μM, 30 min). Co-localization coefficients of **Mito-MOI** and MTG (c) in SiHa and astrocytes. λ_{ex} = 488 nm, λ_{em} = 600-700 nm to **Mito-MOI**, λ_{em} = 490-520 nm to MTG. Bar = 20 μm (the mean ± SD from three independent experiments).

Selectivity to mitochondria. The absorption and fluorescence spectra of **Mito-MOI**, MTG and MTR were studied (Figure S1). When excited by 488 nm, both **Mito-MOI** and MTG emitted fluorescence. If collecting 600-700 nm for **Mito-MOI** and 490-520 nm for MTG, there would not be optical interferences between the two dyes. Thus, co-staining experiment with MTG was carried out to investigate the intracellular localization of **Mito-MOI**.[32] The confocal microscopic photos of SiHa and rat astrocytes incubated with **Mito-MOI** and MTG were shown in Figure 2. The average co-localization coefficients of **Mito-MOI** and MTG in SiHa and astrocytes were 0.93 and 0.95, respectively. These results indicated that **Mito-MOI** was capable of imaging intracellular mitochondria exclusively.

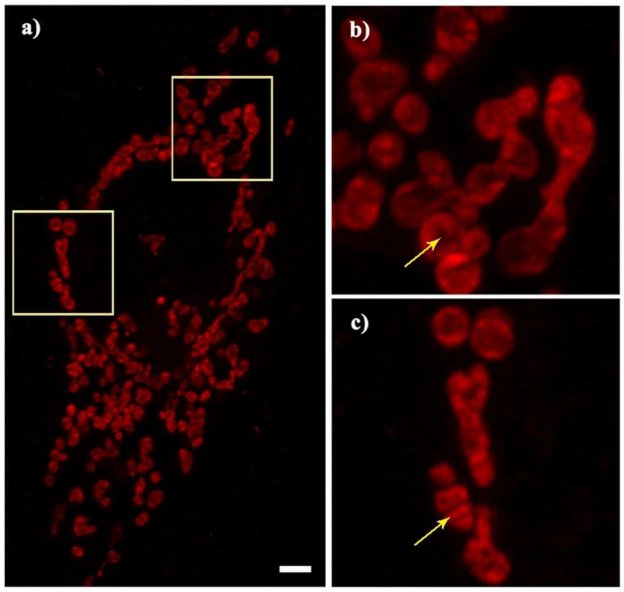

Figure 3. a) Deconvolved high-resolution 3D reconstruction image by Airyscanning in SiHa cells stained with **Mito-MOI** (5 μM, 5 min); b) and c), The enlargement images of the yellow box in (a) and the yellow arrows are pointed to the cristae. λ_{ex} = 488 nm, λ_{em} = 490-700 nm. Bar = 2 μm.

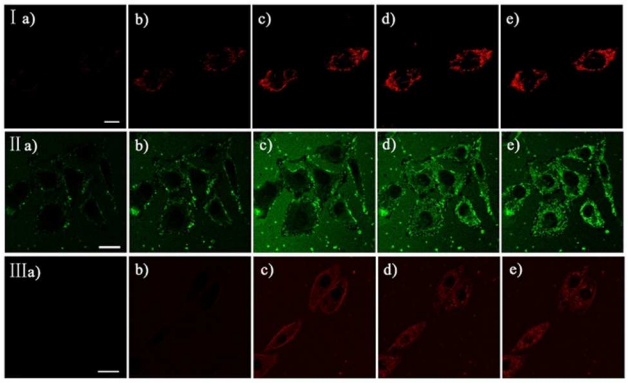

Figure 4. Real-time images of living SiHa cells stained with **Mito-MOI** (I, 5 μM), MTG (II, 0.2 μM), MTR (III, 0.2 μM). The observation time: 3 min (a), 5 min (b), 10 min (c), 20 min (d), 30 min (e). **Mito-MOI** and MTG, λ_{ex} = 488 nm, λ_{em} = 490-700 nm; MTR, λ_{ex} = 561 nm, λ_{em} = 570-700 nm. Bar = 20 μm.

High-resolution imaging mitochondrial inner membrane. In SiHa cells stained with **Mito-MOI**, the deconvolved three-dimensional (3D) reconstruction image (Figure 3) was obtained by Airyscanning. Each individual mitochondrion with oval morphological and hollow structure was imaged without background noise. In the magnified pictures, mitochondria were stained as hollow spheres, indicating that **Mito-MOI** were rich in mitochondrial membrane. Considering that cationic mitochondrial probes were collected by mitochondria due to the negative membrane potential across mitochondrial inner membrane,[19-21] **Mito-MOI** should target the inner membrane. Moreover, the cristae, a characteristic structure of mitochondrial inner membrane (as shown in Figure S2, SEM picture), can be also observed though vague (as marked by yellow arrows in Figure 3b and c). These results further proved that **Mito-MOI** indeed stained mitochondrial inner membrane.

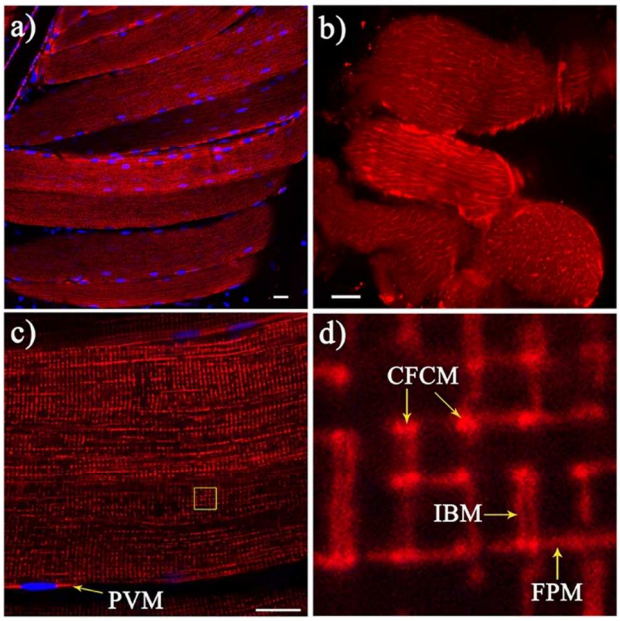

Figure 5. Morphology of mitochondria in skeletal muscle tissue stained with **Mito-MOI** (5 μM, 5 min) and Hoechst 33342 (5 μM, 30 min). a) Confocal fluorescence images of longitudinal plane at 20× magnification; b) Cross-sectional plane at 40× magnification; c) Longitudinal plane at 60× magnification; d) Enlargement of the yellow box in c). **Mito-MOI**, λ_{ex} = 488 nm, λ_{em} = 490-700 nm; Hoechst 33342, λ_{ex} = 405 nm, λ_{em} = 420-470 nm. Bar = 20 μm.

Fast and high-fidelity imaging mitochondria in living cells. SiHa cells were stained with **Mito-MOI**, MTG and MTR for 30 min, respectively. In Figure 4I and Video S1a from **Mito-MOI**, nearly no background signal was observed in cytoplasm and culture medium. Particularly, mitochondria were visualized in less than 5 min. While in Figure 4II and Video S1b, MTG showed intense background noise. Moreover, MTG firstly stained plasma membrane in 5 min and mitochondria were visualized after 20 min. In Figure 4III and Video S1c from MTR, there was still some detectable background noise in culture medium. Similar to MTG, MTR also firstly stained plasma membrane and then stained mitochondria in more than 10 min. These results showed that **Mito-MOI** had fast stainability and could high-fidelity image mitochondria with wash-free procedure, while MTG and MTR cannot. From

spectra of **Mito-MOI**, MTG and MTR in organic solvent and water, the relative intensity ratios of **Mito-MOI** in organic solvents and water were higher than that of MTG and MTR (Figure S3), which proved that **Mito-MOI** had higher signal to noise ratio (SNR).

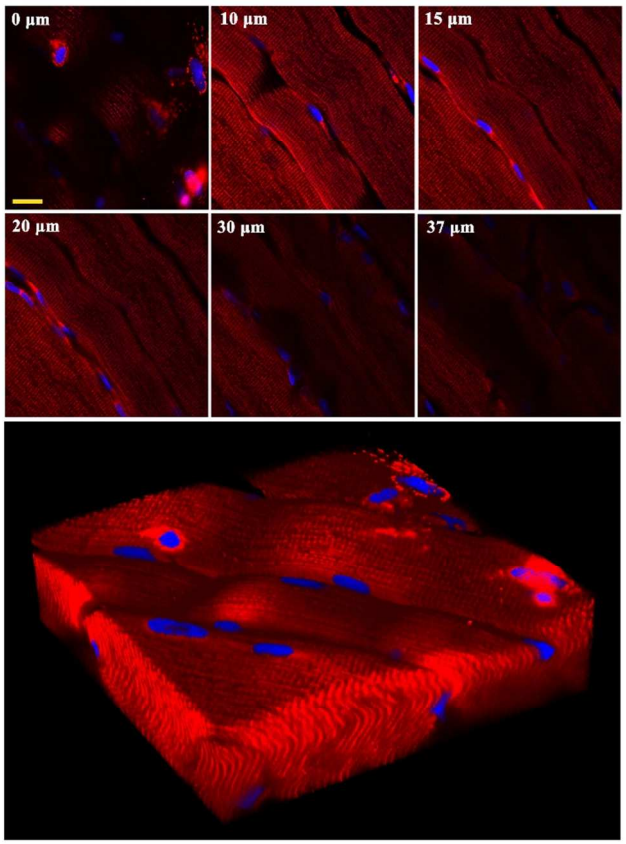

Figure 6. Z-stack images were taken of every 1 μm section from the top to bottom and 3D reconstruction of one muscle tissue (135 μm × 135 μm × 37 μm,) showing spatial relationships between different mitochondria and nucleus. **Mito-MOI**, λ_{ex} = 488 nm, λ_{em} = 490-700 nm; Hoechst 33342, λ_{ex} = 405 nm, λ_{em} = 420-470 nm. Bar = 20 μm.

Fast and high-fidelity imaging mitochondria in living tissues. A piece of skeletal muscle tissue from a seven-week old rat without fixation was stained with **Mito-MOI** and Hoechst 33342 by wash-free procedure. Examination of mitochondrial morphology in both longitudinal and cross-sectional (transverse) planes was achieved by optical sectioning of confocal microscopy. The longitudinal view (Figure 5a) revealed that mitochondria were regularly arranged and formed reticulum in muscle, whereas the transverse view (Figure 5b) revealed the actual tubular morphology of intermyofibrillar (IMF) mitochondria. The results above were consistent with the mitochondrial structure in skeletal muscle obtained by SEM.[33-35] Particularly, four kinds of mitochondria with different morphologies have been *in-situ* observed (Figure 5c and d): paracascular mitochondria (PVM), I-band mitochondria (IBM), fiber parallel mitochondria (FPM), and cross fiber connection mitochondria (CFCM). Four kinds of mitochondria formed crystal-like networks and provided a conductive pathway for skeletal muscle energy distribution.[36,37]

By optical sectioning of the tissue, a series of fluorescent images was captured every 1 μm along the z axis (Figure 6 and S4), and their computer-generated 3D reconstruction images was obtained (Figure 6), which showed a clear intracellular mitochondrial networks and the spatial organization of nucleus and different mitochondria. In addition, we also got cross-sectional images every 1.7 μm along the z axis (Figure S5). The results showed that mitochondria at a 50.9 μm depth can be visualized by **Mito-MOI**.

At the same time, hepatic and myocardial tissues were also studied. According to Figure S6a, mitochondria filled cytoplasm of polygonal hepatocytes. And the staining depth was 40 μm. In Figure S6b, the longitudinal section of the myocardial tissue was shown. Moreover, a staining depth of 36 μm was exciting as myocardial tissue was also denser.

Tracking dynamic process of mitochondrial fission. The variations of the location and orientation of mitochondria were real-time tracked in living rat astrocytes. (Figure 7I, Video S2). In tracking process of 20 min, little intracellular and extracellular background fluorescence was observed, and only mitochondria emitted bright fluorescence. Thus the dynamic process of mitochondrial fission from 480 s to 520 s was shown clearly *in situ*. Delightfully, mitochondrial morphology and distribution in a neuron was also visualized clearly (Figure 7II). In particular, mitochondrial morphology in neuronal soma was clearly shown in the enlargement image.

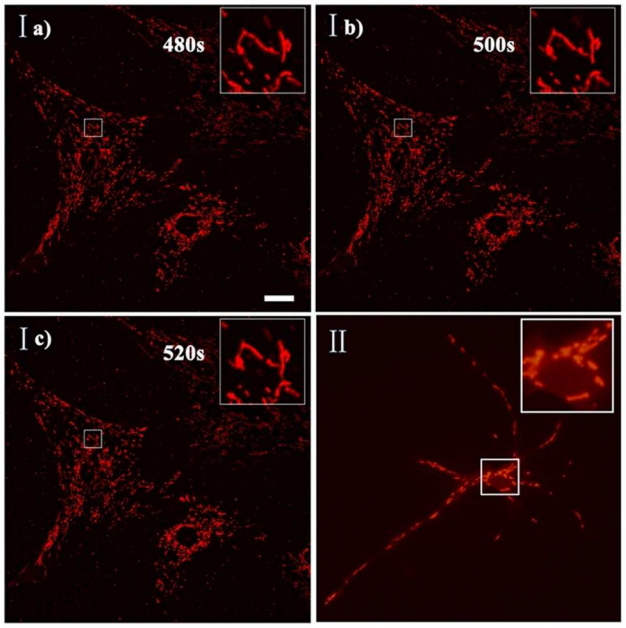

Figure 7. Real-time tracking images of living rat astrocytes (I) and wide-field fluorescence image of living rat neuron (II) stained with **Mito-MOI** (5 μM). Enlargement images from 480 s (Ia) to 520 s (Ic) showing mitochondrial fission. Enlargement image in (II) showing mitochondrial morphology in neuronal soma. I) λ_{ex} = 488 nm, λ_{em} = 490-700 nm; II) λ_{ex} = 510-550 nm, λ_{em} > 570 nm. Bar = 20 μm.

Photostability and other advantages. To quantitatively compare the photostability of **Mito-MOI**, MTG and MTR, one of the most crucial criteria on fluorescent imaging agents,[25, 38-40] HeLa cells stained by them were exposed to constant laser beam. The fluorescence intensity of intracellular dyes was normalized and plotted as a function of time. In Figure 8, **Mito-MOI** exhibited constant fluorescence emission during continuous laser irradiation of 15 min. In contrast, under the same laser intensity, the signal intensity of MTG and MTR decayed sharply in 2 min and 1 min, respectively, indi-

cating the superior photostability of **Mito-MOI**. Moreover, the cytotoxicity of **Mito-MOI** with different concentrations in HeLa and SiHa cells was investigated and the cell viability assay data were quantified. As shown in Figure 9a and b, the viability of HeLa and SiHa cells incubated with 10 μM **Mito-MOI** was more than 85% after incubation for 24 h. Thus the micromolar concentrations of **Mito-MOI** should be nontoxic.

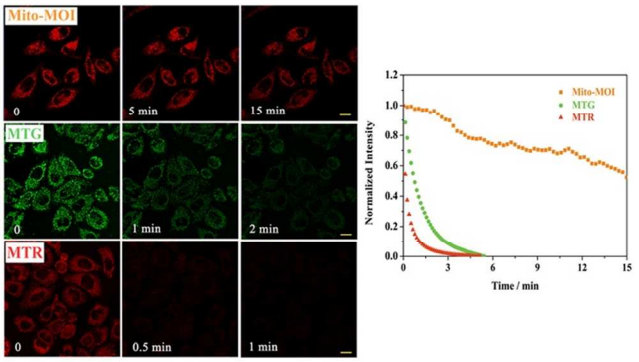

Figure 8. Confocal fluorescence microscopy images (left) of the living HeLa cells incubated with **Mito-MOI** (5 μM, 5 min), MTG (0.2 μM, 30 min), MTR (0.2 μM, 30 min) and photostability comparison was shown in the right figure. **Mito-MOI** and MTG, λ_{ex} = 488 nm, λ_{em} = 490-700 nm; MTR, λ_{ex} = 561 nm, λ_{em} = 570-700 nm. Bar = 20 μm.

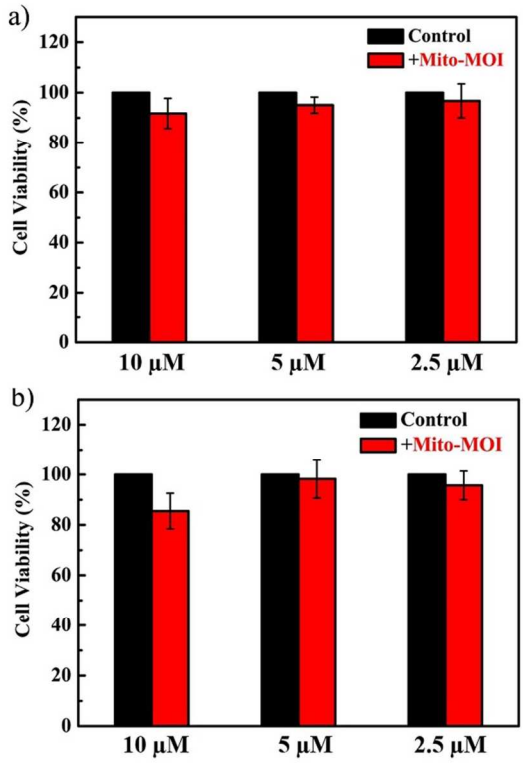

Figure 9. MTT results of HeLa (a) and SiHa (b) cell viabilities after incubation with **Mito-MOI** (10 μM, 5 μM, 2.5 μM) for 24 h.

CONCLUSIONS

To summarize, we have synthesized a phospholipid-biomimetic mitochondrial probe **Mito-MOI** with ultrahigh selectivity due to its dual targeting groups (cation and C_{18}-alkyl chain). As expected, high resolution microscopic photos showed that it stained mitochondrial inner membrane without background noise. Different from conventional mitochondrial probes, **Mito-MOI** had faster stainability, higher SNR and removed washing process. Therefore, high-fidelity mitochondrial fluorescent images in intact living tissues have been successfully obtained. Particularly, four kinds of mitochondria and their crystal-like structure in muscle tissues were visualized clearly. Furthermore, **Mito-MOI** could track the dynamic process of mitochondrial fission and has excellent photostability as well as low toxicity. The strategy of dual targeting groups should have important value for designing probes with ultrahigh selectivity to various intracellular membranous components.

ASSOCIATED CONTENT

Supporting Information

Additional information as noted in text. This material is available free of charge via the Internet at http://pubs.acs.org.

The synthetic details and characterization of **Mito-MOI**, photophysical properties of **Mito-MOI**, SEM imaging of muscle fiber, relative intensity ratio of **Mito-MOI**, MTG and MTR, fluorescent images of optical sectioning of skeletal muscle tissues, confocal fluorescence images of rat hepatic tissue and myocardial tissue. (PDF)

Videos: Real-time observation of living SiHa cells stained with **Mito-MOI**, MTG and MTR, respectively. Real-time tracking of living rat astrocytes stained with **Mito-MOI**. (AVI)

AUTHOR INFORMATION

Corresponding Author

Xiaoqiang Yu
Fax: +86 0531 88364263;
E-mail address: yuxq@sdu.edu.cn

Jing Zhi Sun
Fax: +86 0571 87953734;
E-mail address: sunjz@zju.edu.cn

Xiuquan He
Fax: +86 0531 88364263;
E-mail address: hxq3000@sdu.edu.cn

Notes

The authors declare no competing financial interest.

ACKNOWLEDGMENT

Our Laser confocal scanning imaging of living cells was performed at The Microscopy Characterization Facility, Shandong University. For financial support, we thank the National Natural Science Foundation of China (51273107, 51273175 and 21672130), Natural Science Foundation of Shandong Province, China (ZR2012EMZ001), Shandong University 2011JC006, Open Project of State Key Laboratory for Supramolecular Structure and Materials (SKLSSM201524).

REFERENCES

(1) Zhao, M.; Wan, X. Y.; Li, Y.; Zhou, W. B.; Peng, L. L. *Sci. Rep.* **2015**, *5*, 13991.

(2) Estrada, M. F.; Rebelo, S. P.; Davies, E. J.; Pinto, M. T.; Pereira, H.; Santo, V. E.; Smalley, M. J.; Barry, S. T.; Gualda, E. J.;

Alves, P. M.; Anderson, E.; Brito, C. *Biomaterials* **2016**, *78*, 50-61.
(3) Pampaloni, F.; Reynaud, E. G.; Stelzer, E. H. K. *Nat. Rev. Mol. Cell Biol.* **2007**, *8*, 839-845.
(4) Kleinman, H. K.; Philp, D.; Hoffman, M. P. *Curr. Opin. Biotechnol.* **2003**, *14*, 526-532.
(5) Weaver, V. M.; Petersen, O. W.; Wang, F.; Larabell, C. A.; Briand, P.; Damsky, C.; Bissell M. J. *J. Cell Biol.* **1997**, *137*, 231-245.
(6) Obinata, M. *Cancer Sci.* **2007**, *98*, 275-283.
(7) Vincent, A. E.; Yi, S. N.; White, K.; Davey, T.; Mannella, C.; Falkous, G.; Feeney, C.; Schaefer, A. M.; McFarland, R.; Gorman, G. S.; Taylor, R. W.; Turnbull, D. M.; Picard, M. *Sci. Rep.* **2016**, *6*, 30610.
(8) Rocha, M. C.; Grady, J. P.; Grünewald, A.; Vincent, A.; Dobson, P. F.; Taylor, R. W.; Turnbull, D. M.; Rygiel, K. A. *Sci. Rep.* **2015**, *5*, 15037.
(9) Khan, N. A.; Auranen, M.; Paetau, I.; Pirinen, E.; Euro, L.; Forsström, S.; Pasila, L.; Velagapudi, V.; Carroll, C. J.; Auwerx, J.; Suomalainen, A. *Embo Mol. Med.* **2014**, *6*, 721-731.
(10) Wang, Y.-X.; Le, W.-D. *Chinese Med. J.* **2015**, *128*, 1820-1825.
(11) Sarkar, A. R.; Heo, C. H.; Lee, H. W.; Park, K. H.; Suh, Y. H.; Kim, H. M. *Anal. Chem.* **2014**, *86*, 5638-5641.
(12) Liu, F.; Wu, T.; Cao, J. F.; Cui, S.; Yang, Z. G.; Qiang, X. X.; Sun, S. G.; Song, F. L.; Fan, J. L.; Wang, J. Y.; Peng, X. J. *Chem. Eur. J.* **2013**, *19*, 1548-1553.
(13) Zhang, X. F.; Xiao, Y.; Qi, J. L.; Kim, B.; Yue, X. L.; Belfield, K. D. *J. Org. Chem.* **2013**, *78*, 9153-9160.
(14) Miao, F.; Zhang, W. J.; Sun, Y. M.; Zhang, R. Y.; Liu, Y.; Guo, F. Q.; Song, G. F.; Tian, M. G.; Yu, X. Q. *Biosens. Bioelectron.* **2014**, *55*, 423-429.
(15) Zhang, G.; Sun, Y. M.; He, X. Q.; Zhang, W. J.; Tian, M. G.; Feng, R. Q.; Zhang, R. Y.; Li, X. C.; Guo, L. F.; Yu, X. Q.; Zhang, S. L. *Anal. Chem.* **2015**, *87*, 12088-12095.
(16) Huang, Y.; Yu, F. B.; Wang, J. C.; Chen, L. X. *Anal. Chem.* **2016**, *88*, 4122-4129.
(17) Park, S.; Bae, D. J.; Ryu, Y.-M.; Kim, S.-Y.; Myung, S.-J.; Kim, H.-J. *Chem. Commun*. **2016**, *52*, 10400-10402.
(18) Gao, M.; Yu, F. B.; Chen, H.; Chen, L. X. *Anal. Chem.* **2015**, *87*, 3631-3638.
(19) Mehto, R.; Kumar, N.; Bhalla, V.; Kumar, M. *Chem. Commun.* **2015**, *51*, 15614-15628.
(20) Jean, S. R.; Ahmed, M.; Lei, E. K.; Wisnovsky, S. P.; Kelley, S. O. *Acc. Chem. Res.* **2016**, *49*, 1893-1902.
(21) Liu, Y.; Zhou, J.; Wang, L. L.; Hu, X. X.; Liu, X. J.; Liu, M. R.; Cao, Z. H.; Shangguan, D. H.; Tan, W. H. *J. Am. Chem. Soc.* **2016**, *138*, 12368-12374.
(22) Liu, B.; Shah, M.; Zhang, G.; Liu, Q.; Pang, Y. *ACS Appl. Mater. Interfaces* **2014**, *6*, 21638-21644.
(23) Mizukami, S.; Watanabe, S.; Akimoto, Y.; Kikuchi, K. *J. Am. Chem. Soc.* **2012**, *134*, 1623-1629.
(24) Hori, Y.; Norinobu, T.; Sato, M.; Arita, K.; Shirakawa, M. *J. Am. Chem. Soc.* **2013**, *135*, 12360-12365.
(25) Leung, C. W.; Hong, Y. N.; Chen, S. J.; Zhao, E. G.; Lam, J. W.; Tang, B. Z. *J. Am. Chem. Soc.* **2013**, *135*, 62-65.
(26) Kim, C. Y.; Kang, H. J.; Chung, S. J.; Kim, H.-K.; Na, S.-Y.; Kim, H.-J. *Anal. Chem.* **2016**, *88*, 7178-7182.
(27) Lim, S.-Y.; Hong, K.-H.; Kim, D. I.; Kwon, H.; Kim, H.-J. *J. Am. Chem. Soc.* **2014**, *136*, 7018-7025.
(28) Ross, M. F.; Kelso, G. F.; Blaikie, F. H.; James, A. M.; Cochemé, H. M.; Filipovska, A.; Da Ros, T.; Hurd, T. R.; Smith, R. A. J.; Murphy, M. P. *Biochemistry* **2005**, *70*, 222-230.
(29) Krumova, K.; Greene, L. E.; Cosa, G. *J. Am. Chem. Soc.* **2013**, *135*, 17135-17143.
(30) Klymchenko, A. S.; Kreder, R. *Chem. Biol.* **2013**, *21*, 97-113.
(31) Feng, R. Q.; Sun, Y. M.; Tian, M. G.; Zhang, G.; Zhang, R. Y.; Guo, L. F.; Li, X. C.; Yu, X. Q.; Zhao, N. *J. Mater. Chem. B* **2015**, *3*, 8644-8649.
(32) Yu, F. B.; Gao, M.; Li, M.; Chen, L. X. *Biomaterials* **2015**, *63*, 93-101.
(33) Ogata, T.; Yamasaki, Y. *Anat. Rec.* **1997**, *248*, 214-223.
(34) Dahl, R.; Larsen, S.; Dohlmann, T. L.; Qvortrup, K.; Helge, J. W.; Dela, F.; Prats, C. *Acta Physiol.* **2015**, *213*, 145-155.
(35) Picard, M.; Gentil, B. J.; McManus, M. J.; White, K.; St. L. K.; Gartside, S. E.; Wallace, D. C.; Turnbull, D. M. *J. Appl. Physiol.* **2013**, *115*, 1562-1571.
(36) Vendelin, M.; Béraud, N.; Guerrero, K.; Andrienko, T.; Kuznetsov, A. V.; Olivares, J.; Kay, L.; Saks, V. A. *Am. J. Physiol. Cell Physiol.* **2005**, *288*, C757-C767.
(37) Glancy, B.; Hartnell, L. M.; Malide, D.; Yu, Z.-X.; Combs, C. A.; Connelly, P. S.; Subramaniam, S.; Balaban, R. S. *Nature* **2015**, *523*, 617-620.
(38) Liu, X. G.; Qiao, Q. L.; Tian, W. M.; Liu, W. J.; Chen, J.; Lang, M. J.; Xu, Z. C. *J. Am. Chem. Soc.* **2016**, 138, 6960-6963.
(39) Song, G. F.; Sun, Y. M.; Liu, Y.; Wang, X. K.; Chen, M. L.; Miao, F.; Zhang, W. J.; Yu, X. Q.; Jin, J. L. *Biomaterials* **2014**, *35*, 2103-2112.
(40) Jiang, N.; Fan, J. L.; Xu, F.; Peng, X. J.; Mu, H. Y.; Wang, J. Y.; Xiong, X. Q. *Angew. Chem. Int. Ed.* **2015**, *54*, 2510-2514.

Table of Contents (TOC):